Journal of Computational Chemistry

WILEY

Journal of COMPUTATIONAL CHEMISTRY

RESEARCH ARTICLE

Generalized Turnstile Rotation: Formulation, Visualization, Workflow Implementation, and Application for Modeling Polytopal Rearrangements

Yunwen Tao[1] | Xianlong Wang[2] | Wenli Zou[3] | Elfi Kraka[4]

[1]Independent Researcher, Arlington, Texas, USA | [2]Department of Bioinformatics, School of Medical Technology and Engineering, Fujian Medical University, Fuzhou, People's Republic of China | [3]Institute of Modern Physics, Northwest University, Xi'an, Shaanxi, People's Republic of China | [4]Department of Chemistry, Southern Methodist University, Dallas, Texas, USA

Correspondence: Yunwen Tao (ywtao.smu@gmail.com) | Elfi Kraka (ekraka@smu.edu)

Received: 24 April 2026 | **Revised:** 24 April 2026 | **Accepted:** 26 May 2026

ABSTRACT

Turnstile rotation is a well-known polytopal rearrangement mechanism in coordination compounds, yet its computational description is often hindered by the challenges of conventional internal coordinates to represent such collective, large-amplitude motions. In this work, we present a mathematical formulation for generalized *N*-arm turnstile rotation, a dedicated PyMOL plugin (gTA) for intuitive structure visualization and a command-line utility (gTA-cli) for structure manipulation. On this basis, we develop a practical computational workflow that combines turnstile rotation-driven relaxed scans with two downstream routes to locate the transition states. The generality of the approach is demonstrated through five chemically diverse case studies, ranging from classical rearrangements in SF_4, IF_7, and $[Co(en)_3]^{3+}$ to previously unexplored fluxional processes in bismuth and nickel complexes. In all cases, the method enables the identification of transition states associated with pronounced polytopal rearrangements that are difficult to access using standard coordinate schemes. These results establish generalized turnstile rotation as a fundamental molecular motion and highlight its potential as a broadly applicable strategy for studying fluxionality and dynamic stereochemistry in coordination chemistry. The PyMOL plugin gTA and the Python utility gTA-cli with the associated relaxed scan workflows are open-source and freely available on Github at https://github.com/smutao/gTA-plugin and https://github.com/smutao/gTA-workflow, respectively.

1 | Introduction

The accurate computational description of large-amplitude, collective rearrangements remains a central challenge in the study of fluxional coordination compounds. Many stereochemical interconversions in main-group and transition-metal complexes involve concerted ligand motions that cannot be naturally expressed in terms of simple bond-length, bond-angle, or dihedral-angle distortions. As a consequence, identifying appropriate reaction coordinates with relaxed scans and transition state (TS) searches often becomes nontrivial, limiting the practical exploration of complex polytopal rearrangements using standard quantum-chemical tools.

One representative class of such collective motions is the *turnstile rotation*, a type of *polytopal rearrangement* [1, 2] encountered in coordination compounds.

The concept was first introduced in 1971 by Ugi, Ramirez, and coworkers to describe an isomerization mechanism in which five ligating atoms partition into a two-membered pair (one apical, one equatorial) and a three-membered trio (the remaining ligands) [3, 4]. These two subsets undergo a coordinated internal rotation of approximately 60° relative to each other, functioning analogously to a mechanical turnstile and enabling positional exchange. This model provided an explanation for rapid stereoisomerization in constrained polycyclic

TABLE 1 | Comparison of polytopal rearrangement mechanisms relevent to turnstile rotation.

Polytopal rearrangement	Example compound	Coordination number	Turnstile arm atoms	Modeled via internal coordinates?[a]
Lever mechanism	SF_4	4	3	Possible[b]
Bartell mechanism	IF_7	7	2	Not clear
Bailar twist	Λ-$Ga^{III}(mda)_3$	6	3	Not clear
Ray-Dutt twist	Λ-$Ga^{III}(mda)_3$	6	2[c]	Not clear
Muetterties M2	Spirocyclic pentaorganylsilicate	5	3	Yes
Muetterties M3	Caged phosphorane	5	2	Yes
Circle dance mechanism	K_2ReH_9 solid	9	5	Possible[d]

[a]Via conventional internal coordinates.
[b]Possibly achievable using augmented internal coordinates with auxiliary dummy atoms; we have not identified a published SF_4 example.
[c]With two turnstiles.
[d]With interpolation of Cartesian coordinates.

phosphoranes, where alternative mechanisms such as Berry pseudorotation (BPR) would require energetically unfavorable intermediates.

Subsequent theoretical developments refined this mechanistic picture. In 2010, Couzijn and coworkers revisited the stereomutation landscape using density functional theory (DFT) combined with internal coordinate analysis [5]. They demonstrated that Ugi's original turnstile rotation is topologically equivalent to BPR when overall molecular reorientation is neglected. Instead, they identified two higher-order concerted mechanisms, denoted M2 and M3, which proceed via multiple Berry-type deformations. The M2 mechanism corresponds to a threefold cyclic permutation involving an effective 120° rotation and closely resembles a mechanical three-arm turnstile, whereas the M3 mechanism corresponds to a 180° two-arm turnstile rotation composed of three consecutive Berry motions. On this basis, the term "turnstile rotation" was reassigned specifically to the M2 pathway.

Beyond these prototypical systems, turnstile-like motions have been identified in a broad range of fluxional processes. Our recent theoretical studies of rhenium polyhydride complexes $ReH_5(PPh_3)_2(py)$ and ReH_9^{2-} revealed turnstile rotation mechanisms operative in both solution and crystalline environments [6, 7]. Similar fluxional behavior was later observed in related Re–NHC polyhydride systems by Grieco and co-workers [8]. Moreover, several other well-known polytopal rearrangements, including Bailar and Ray–Dutt twists in hexacoordinate trischelates, the Bartell mechanism in iodine heptafluoride (IF_7), and the lever mechanism in sulfur tetrafluoride (SF_4), exhibit reaction pathways that are closely related to turnstile-type collective motions (see Table 1) [5, 9]. Taken together, these observations suggest that turnstile rotation represents a broadly relevant class of molecular motion rather than a narrowly defined mechanistic special case.

Despite its apparent prevalence, the molecular modeling of turnstile rotation remains challenging within standard computational chemistry workflows. A central difficulty lies in the absence of reaction coordinates specifically designed to describe this type of concerted polytopal rearrangement. Conventional internal coordinates including bond lengths, bond angles, dihedral angles, and out-of-plane torsions, do not provide a intuitive or generally applicable representation of turnstile rotation. As a result, relaxed scans often rely on ad hoc combinations of multiple coordinates, and the systematic identification of TSs associated with such motions becomes inefficient or unreliable. Although the adoption of dummy atoms may serve as a workaround in certain cases (e.g., the lever mechanism in SF_4), such approaches require expert knowledge of the Z-matrix formalism and are difficult to be generalized and automated. A dedicated structure parameter tailored explicitly to turnstile rotation would therefore be of substantial practical value for exploring complex rearrangement mechanisms.

In our previous work, we developed a curvilinear coordinate system for describing polytopal rearrangements based on displacements along vibrational normal modes [2]. This framework is applicable to coordination compounds ranging from tetra- to hepta-coordinate geometries and spans the complete configuration space of the first coordination sphere AB_n. Its implementation in an in-house version of the Gaussian package [10] enables relaxed scans using these curvilinear coordinates for the central AB_n motif, combined with a Z-matrix description of the outer-layer atoms. Related approaches have been proposed by Canfield, Crossley, and coworkers, who employed angle-changing vibrational normal modes under the assumption of rigid bonds to generate an orthonormal basis spanning the stereoisomeric configuration space [11, 12]. Nevertheless, when applied specifically to turnstile rotation, these normal-mode-based approaches require the prudent selection and combination of multiple vibrational modes, and the resulting reaction coordinates are neither unique nor intuitive. This practical ambiguity limits their routine use in relaxed scans and complicates the systematic location of TSs associated with turnstile-type rearrangements. More generally, the lack of a single, well-defined coordinate that directly encodes turnstile rotation has hindered the development of transferable and efficient workflows for studying such collective motions.

Motivated by these limitations, we introduce *generalized turnstile rotation* as an elementary collective motion that can be expressed as a standalone, mathematically explicit coordinate. This formulation enables turnstile rotation to be driven directly in relaxed scans, providing a controlled and chemically transparent pathway for exploring complex polytopal rearrangements.

The paper is organized as follows. We first present the mathematical formulation of generalized turnstile rotation and then describe its implementation in two complementary tools: a PyMOL plugin for intuitive motion visualization and molecular structure editing, and a Python utility program for scriptable structure manipulation and workflow integration. We next introduce a turnstile rotation-driven relaxed scan workflow and demonstrate its performance across five representative case studies encompassing both classical and previously unexplored fluxional processes. These examples illustrate how the proposed methodology facilitates the systematic identification of TSs associated with large-amplitude polytopal rearrangements. Computational details are provided thereafter, and the main conclusions are summarized in the final section.

2 | Formulation

For an N-arm turnstile commonly seen in real life where N is usually 3 (see Figure 1), all arms have identical length and they rotate around an invisible C_N axis with the interval of $360/N$ degrees. The endpoints of these N arms lie on a circle, and these N points divide the circle into N equal arcs.

However, the turnstile-like geometry in a coordination compound is not guaranteed to fulfill the above requirements. Therefore, we provide the formulation for the generalized N-arm turnstile rotation in this section.

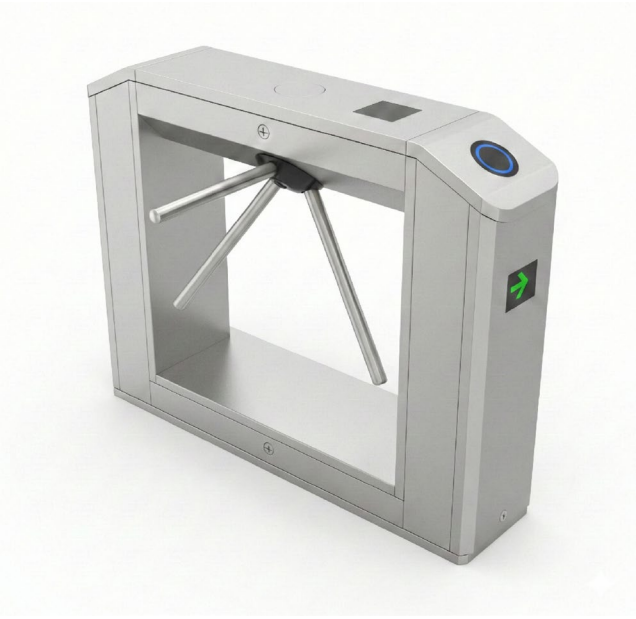

FIGURE 1 | Photo of a three-arm turnstile. This image was generated by Gemini Nano Banana model.

Given the central atom and N ligating atoms participating in the turnstile rotation in a coordination compound, the essence of defining such a turnstile rotation lies in specifying the rotation axis passing the central atom. To determine this axis, we provide an explicit mathematical formulation as follows and the schematic illustration is provided in Figure 2.

If there are N atoms bonded to the central atom O collectively forming a N-arm turnstile rotation. These N atoms are labeled with $A_1, A_2, \ldots, A_N$ (i.e., $\{A_i\}_{i=1}^{N}$ where $N \geq 3$) consecutively in a clockwise or anticlockwise manner. We need to note that in real molecular structures, the distances $\|\mathbf{O}-\mathbf{A_i}\|$ and angles $\angle A_i O A_{i+1}$ are not necessarily identical for different i.

Starting from point O, the point R_i is constructed by extending the ray toward A_i and selecting the point at a fixed distance D from point O (i.e., $\|\mathbf{R_i}-\mathbf{O}\| = D$). This distance D is chosen arbitrarily but kept the same for each i through 1 to N.

Given the point O and an unknown point Q, the line through Q and O uniquely defines a plane passing through Q and orthogonal to this line. Within this plane, a circle centered at Q with radius r is constructed. On this circle, N points $\{F_i\}_{i=1}^{N}$ are placed at equal angular intervals according to an implicit phase angle $\phi \in (0, 2\pi]$. The point Q, the radius r and the phase angle ϕ are then determined by minimizing the sum of squared distances between the points F_i and the corresponding points R_i, that is,

$$(Q^*, r^*, \phi^*) = \underset{Q,r,\phi}{\arg\min} \sum_{i=1}^{N} \|\mathbf{F}_i - \mathbf{R}_i\|^2 \tag{1}$$

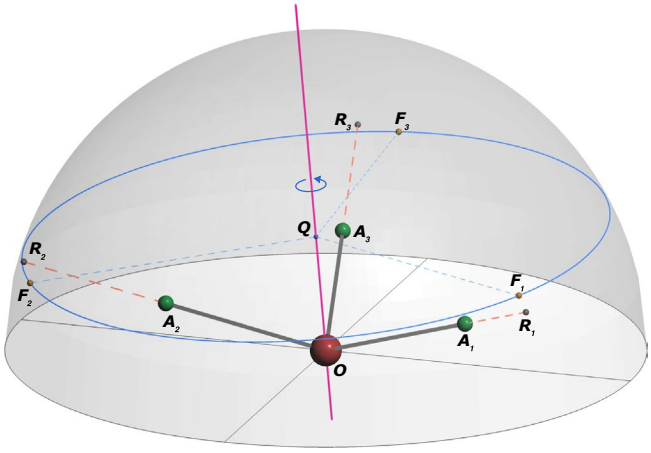

FIGURE 2 | Schematic illustration for the definition of generalized N-arm turnstile rotation in $N = 3$ case. The atom O is defined as the origin and 3 atoms A_i ($i = 1,2,3$) are bonded to the central atom O. Each point R_i lies on the extension of the line segment from O to A_i, at a fixed distance from O, which is identical for all i. This semisphere with point O as the center uses the above-mentioned fixed distance as the radius. Point Q is determined by minimizing the sum of squared distances between a set of equally spaced points F_i (which are not necessarily on the semisphere) on a circle centered at Q and the given points R_i, where the circle lies in the plane orthogonal to the line through Q and O. This line (colored in magenta) is then used as the axis for turnstile rotation.

Then this line $\overline{OQ}$ is defined as the axis for the turnstile rotation of the given set of atoms $\{A_i\}_{i=1}^{N}$. Noteworthy is that this axis of rotation is unchanged no matter how much the turnstile rotates.

For the case of $N = 2$, point $\{F_i\}_{i=1}^{2}$ is defined as point $\{R_i\}_{i=1}^{2}$ so that point Q lies on the angle bisector of $\angle R_1 O R_2$.

One may ask why the auxiliary points $\{F_i\}_{i=1}^{N}$ are introduced rather than determining Q directly from the given points $\{R_i\}_{i=1}^{N}$, for example by minimizing the sum of distances or squared distances between Q and the R_i points. Such a direct minimization would merely define a best-fit center for the set $\{R_i\}_{i=1}^{N}$ and would not explicitly encode the defining symmetry of an ideal N-arm turnstile. In contrast, the present formulation determines Q by fitting $\{R_i\}_{i=1}^{N}$ to a set of equally spaced points on a circle lying in the plane perpendicular to $\overline{OQ}$. In this way, the cyclic symmetry of the turnstile is built directly into the optimization problem rather than inferred indirectly from a point cloud.

This choice is also physically reasonable. Although real molecular structures are generally distorted, the ligating atoms participating in a turnstile rotation are still expected to distribute around the rotation axis in an approximately uniform angular fashion because of short-range interligand repulsion. Therefore, the circle with equally spaced $\{F_i\}_{i=1}^{N}$ serves as a natural reference geometry rather than an artificial constraint. Conceptually related constructions have been used in the formulation of ring deformation coordinates for Jahn–Teller-type distortions, where molecular deformations are defined with respect to a regular N-gon reference geometry [13]. In the present context, the introduction of $\{F_i\}_{i=1}^{N}$ provides a similarly symmetric and mathematically transparent reference for defining generalized turnstile rotation.

3 | PyMOL Plugin for Visualizing Turnstile Rotation

In this work, we have developed a user-friendly PyMOL [14, 15] plugin `gTA` (abbreviated for generalized Turnstile Assistant) to help visualize generalized N-arm turnstile rotation formulated in the last section.

After loading the molecular structure of a coordination complex into PyMOL program, we can visualize the turnstile rotation and conduct the structure editing in the following steps:

- Launch the `gTA` plugin in PyMOL software
- Click the `Start` button in the gTA GUI window (see Figure 3)
- Use mouse to click on the central atom (also called *anchor* in this plugin) in the PyMOL viewer area
- Use mouse to click on a turnstile arm atom (i.e., the atom chemically bonded to the central atom), then click `Arm Atom Selection Done` button in the PyMOL wizard menu
- Repeat last step until all N arm atoms have been selected in clockwise/anticlockwise order
- Click the `Picking Finished` button within the gTA GUI window
- Use the slider to adjust the turnstile rotation angle (which is defined by taking the initial structure as the reference)

It is worth noting that all of the ligand atoms participating in the turnstile rotation are automatically inferred based on connectivity information although only the ligating arm atoms are selected via mouse clicks.

The source code for this plugin is available at https://github.com/smutao/gTA-plugin.

4 | Python Utility Program for Modeling Turnstile Rotation

In addition to the PyMOL plugin, we have also developed a Python utility program `gTA-cli` (abbreviated for command-line interface for generalized Turnstile Assistant).

While the PyMOL plugin is convenient for interactive visualization and manual structure editing, it is not ideally suited for tasks that require reproducibility, batch processing, or direct integration into automated computational workflows. In particular, repeated generation of turnstile-rotated structures at many consecutive angles is cumbersome in a graphical environment and difficult to incorporate into script-based quantum-chemical studies. To address these limitations, `gTA-cli` provides a non-interactive implementation of the same generalized turnstile rotation formalism in a command-line environment.

The utility accepts a molecular structure file together with user-defined turnstile specifications, including the central atom, the ordered set of arm atoms, and the desired rotation angle. In this way, it reproduces the core functionalities of the PyMOL plugin without manual intervention. In addition, `gTA-cli` offers several features that are particularly useful in computational practice. First, it can generate a series of output structures corresponding to multiple rotation angles in a single run, which is advantageous for constructing scan trajectories or preparing structure ensembles. Second, it supports the simultaneous application of multiple turnstile rotations within one molecule, provided that no overlap exists among the arm atoms assigned to different turnstiles. Third, the rotation can be applied either to the arm atoms alone, corresponding to a first-coordination-sphere treatment, or to the arm atoms together with all atoms connected to them, thereby enabling rigid-fragment-like manipulation of entire ligand substructures.

These capabilities make `gTA-cli` a practical bridge between the conceptual definition of generalized turnstile rotation and its routine use in molecular modeling. In the present work, this utility serves as the structure-generation engine for the turnstile rotation-driven relaxed scan workflow described in the following section. More generally, its scriptable design makes it suitable for high-throughput exploration of fluxional pathways, automated generation of constrained optimization inputs, and

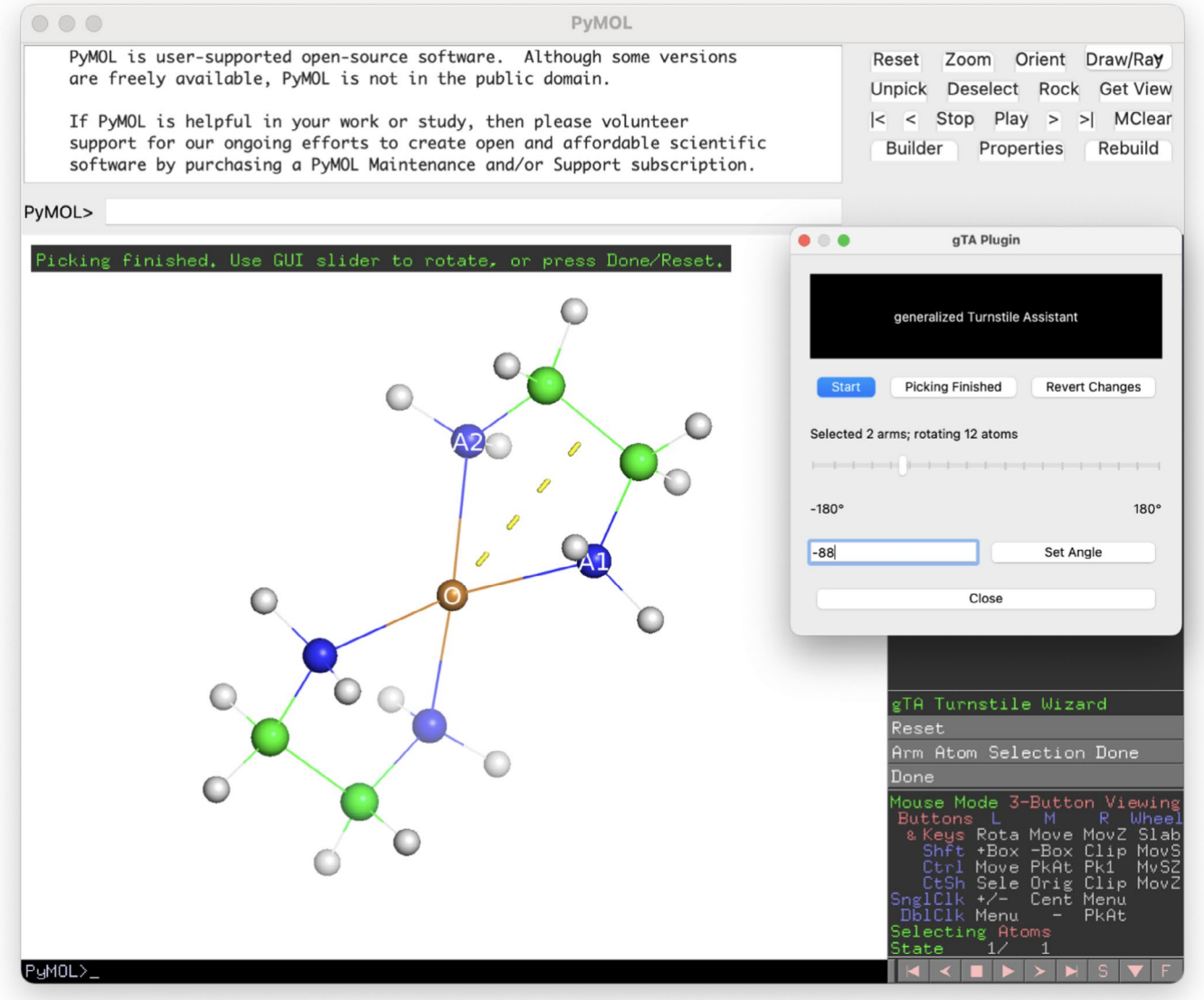

FIGURE 3 | The gTA PyMOL plugin including a graphical user interface (GUI) window and wizard interface.

systematic studies of polytopal rearrangements in chemically diverse coordination compounds.

The source code for this utility is available at https://github.com/smutao/gTA-workflow.

5 | Workflow for Turnstile Rotation-Driven Relaxed Scan and Downstream Routes for Finding TS

As demonstrated in our previous studies, [6, 7] turnstile rotation is a fluxional process that can be investigated theoretically using quantum-chemical calculations to assess the plausibility of proposed mechanisms and to interpret experimental observations, such as NMR data. A central challenge in modeling turnstile rotation, as well as other fluxional rearrangements, is the identification of the TS structure connecting the reactant and product minima. In practical computational studies, reaction pathways are often explored using the coordinate-driving approach, [16–21] in which a relaxed scan is performed along selected internal coordinates. Such scans provide an approximate reaction pathway and allow the identification of an approximate transition state (aTS) as the saddle point on the scanned energy profile. The resulting aTS geometry can then be used as an initial guess for locating the real transition state (rTS), defined as a first-order saddle point on the potential energy surface (PES).

In this work, we introduce a dedicated workflow for turnstile rotation–driven relaxed scans aimed specifically at the efficient generation of aTS structures (Figure 4). In conventional relaxed scan protocols implemented in mainstream quantum chemistry packages, one or two internal coordinates (e.g., bond lengths, bond angles, or dihedral angles) are selected as scan variables while all remaining degrees of freedom are optimized. However, for turnstile rotation, such a treatment is not directly applicable. Our formulation of generalized turnstile rotation defines a relative rotation angle rather than an absolute internal coordinate, necessitating the use of constrained geometry optimization (also referred to as frozen-atom optimization) to emulate a relaxed scan.

Within the proposed workflow (see Figure 4), each step of the relaxed scan consists of two sequential operations. First, an *N*-arm

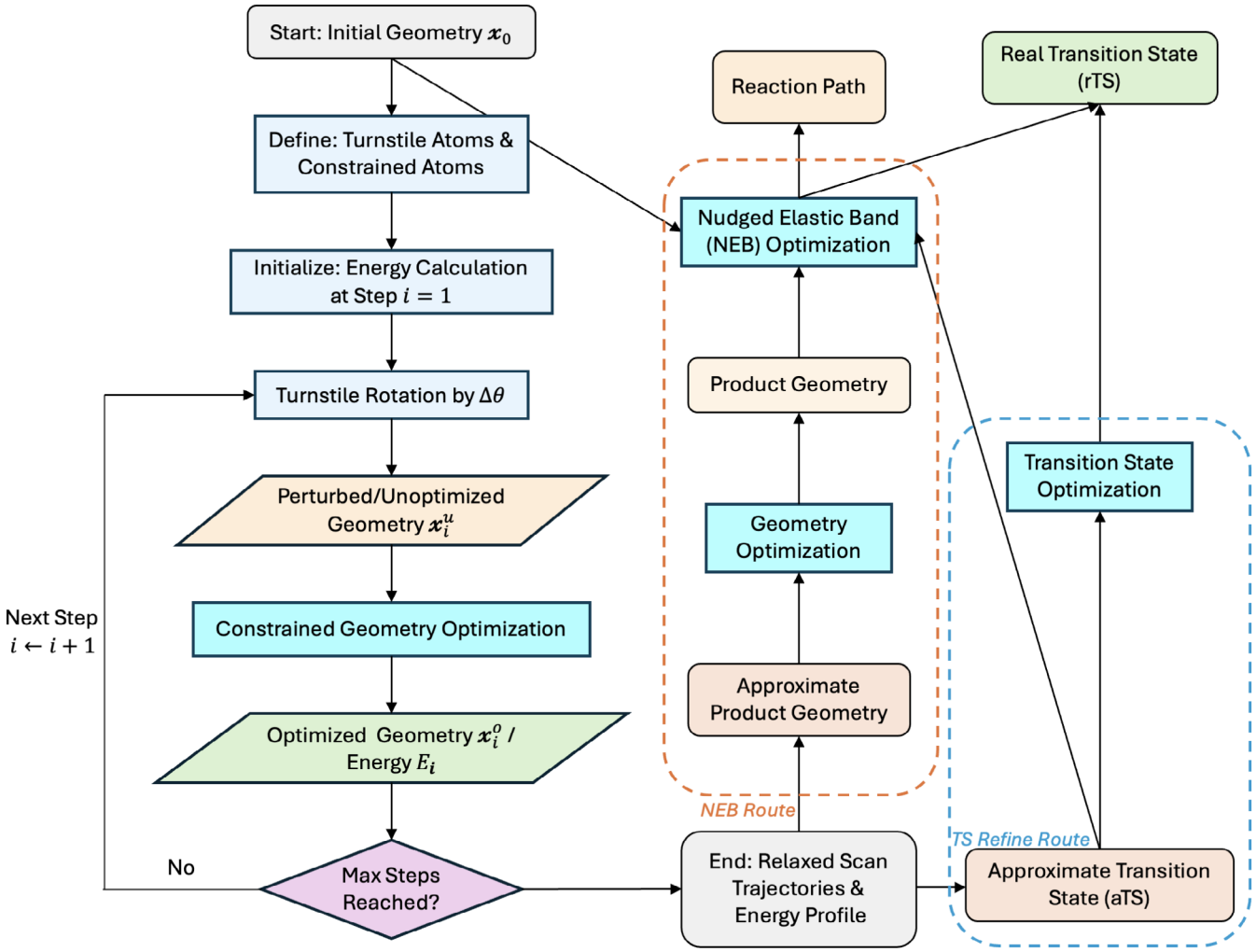

FIGURE 4 | Flowchart of the workflow for turnstile rotation driven relaxed scan (left panel), along with the downstream TS refinement and NEB routes (right panel).

turnstile rotation is applied by incrementing the rotation angle by a small amount $\Delta\theta$ (typically 5°), where N denotes the number of ligating atoms involved ($N \geq 2$). This operation is performed using the utility Python program `gTA-cli` leading to a perturbed geometry. Second, a constrained geometry optimization is carried out in which the Cartesian coordinates of selected atoms within the first coordination sphere are held fixed. It is important to note that freezing only the rotated N-arm ligating atoms during the constrained optimization is insufficient, as this can lead to an overall rigid-body rotation of the molecule. In order to speed up the calculation (especially for large coordination complexes), we may employ some technical tricks like using loose convergence criteria and fixed cycle numbers for geometry optimization to avoid expensive force evaluations in this constrained optimization step. The above-mentioned two sub-steps are repeated a predefined number of times and the optimized geometry from prior step is used as the updated starting geometry for the next step.

The output of this workflow includes the relaxed scan trajectories and the corresponding energy profile from which the aTS point can be easily identified as the local maxima point. If the number of scan steps is large enough, a trough point after aTS is considered as the approximate product geometry.

Such relaxed scan treats the turnstile structure as a rigid body and ignores the potential geometrical strain (induced by turnstile rotation) within the first coordination sphere. We believe that this additional strain energy can be subsequently relieved during geometry relaxation in downstream routes.

A key advantage of the proposed relaxed scan workflow is its ease of implementation. Unlike our previous approach, [2] it does not require modification of the source code of quantum chemistry packages (e.g., the calculation of Wilson B-matrix for the new geometry parameter) and can therefore be readily interfaced with existing electronic-structure methods. This flexibility also opens the door to integrating machine learning potentials (MLPs) into the exploration of turnstile rotation mechanisms. All scripts required to perform the workflow are provided and interfaced with the xTB [22] and ORCA [23] programs. They are available on GitHub at https://github.com/smutao/gTA-workflow.

Following the relaxed scan, two downstream routes can be employed to locate the rTS, as illustrated in the right panel of Figure 4. The first route is direct transition-state refinement starting from the aTS geometry identified on the scan profile. In standard quantum-chemical packages, transition-state

optimization is typically carried out using an eigenvector-following strategy; for example, in ORCA this is implemented through a partitioned rational function optimization (P-RFO) step using an initial TS guess [24]. If successful, this procedure yields the rTS as a first-order saddle point on the PES. To improve the robustness of the optimization, it is often necessary to recompute the Hessian matrix during the optimization, which can become computationally demanding for medium-sized and large systems. Moreover, this direct refinement route is not guaranteed to succeed in every case, because the aTS structure generated by the present relaxed scan still reflects the influence of additional positional constraints beyond the turnstile rotation itself.

As a more robust alternative, we employ a second route based on the nudged elastic band (NEB) method [25]. Compared with direct TS refinement, this route requires two additional structures: the initial geometry used to start the relaxed scan and a product geometry obtained by further optimization of the approximate product structure identified from the scan trajectory. Together with the aTS structure as the TS guess, these geometries define the endpoints and an internal reference for the NEB calculation. In principle, one might argue that the aTS structure is unnecessary for the NEB route and that the two endpoint structures alone should suffice. However, according to our tests, the image-dependent pair potential (IDPP) procedure used to generate the initial NEB path can fail for two-arm turnstile rotation processes in which the initial and final structures differ by an approximately 180° rotation of a ligand. In such cases, IDPP is unable to provide suitable interpolated images unless the aTS geometry is supplied as an internal TS guess. In its climbing-image implementation, the NEB method can locate a candidate rTS with a higher success rate, while avoiding repeated Hessian calculations because only forces on the image structures are required during the optimization. Nevertheless, the resulting TS candidate should still be confirmed by subsequent harmonic vibrational analysis to verify that it corresponds to a true first-order saddle point.

An additional benefit of the NEB route is that the optimized chain of images provides an approximate minimum-energy reaction path for the polytopal rearrangement. This information is useful not only for locating the rTS structure, but also for analyzing the overall progression of the fluxional motion in structural terms. For these reasons, the NEB route becomes the preferred option when direct TS refinement from the aTS structure fails or when the system size renders repeated Hessian evaluations prohibitively expensive.

6 | Application in Modeling Turnstile Rotation Mechanisms

In the following, the application of the workflow proposed in the last section is showcased in detail. We investigated five chemically diverse molecular systems, ranging from previously reported fluxional mechanisms to previously unexplored rearrangements, with the help of generalized turnstile rotation to identify approximate TS structures along the relaxed scan energy profile.

6.1 | Lever Mechanism of Sulfur Tetrafluoride (SF_4)

The lever mechanism in SF_4 molecule is an important fluxional mechanism in additional to the well-known BPR [26]. However, to find the TS structure of lever mechanism is technically challenging due to the complicated PES where three TS points for lever mechanisms surrounds a second-order saddle point according to our previous study with the help of a dedicated curvilinear coordinate system [2, 27]. After careful inspection of the reaction path for lever mechanism, we realize that this fluxional mechanism can be simplified as a three-arm turnstile rotation and the relaxed scan workflow introduced in this work can be applied to find the TS structure starting from the reactant structure.

As shown in Figure 5, we select three F atoms along with the central S atom as the three-arm turnstile motif, and use all four F atoms in the geometry constraint. We use 5° as the step size for the relaxed scan. The energy profile of relaxed scan shows a saddle point (aTS) at step 15 and the structure at step 26 is very similar to the starting structure regardless of the atom permutation.

By using the aTS structure as the initial guess, we successfully obtained the rTS structure with DFT calculations. Further structure alignment for aTS and rTS (see Figure 6) demonstrates high similarity.

6.2 | Bartell Mechanism of Iodine Heptafluoride (IF_7)

The Bartell mechanism in iodine heptafluoride is a classical example of heptacoordinate fluxionality [28]. In structural terms, this rearrangement is dominated by the twisting of two neighboring fluorine atoms in the equatorial plane of IF_7, which can be straightforwardly modeled as a two-arm turnstile rotation. Such a description naturally captures the positional interchange of the two equatorial fluorine atoms and therefore provides a suitable test case for the workflow proposed in this work.

As shown in Figure 7, we selected the two rotating fluorine atoms labeled with 1 and 2 as the turnstile atoms. During the constrained optimization following each turnstile rotation step, these two atoms together with the other two fluorine atoms in the equatorial plane labeled with 3 and 4 were fixed. The relaxed scan was performed with a step size of 5° per step. The resulting energy profile is smooth and leads to a well-defined aTS point. By refining this aTS structure, we successfully identified the rTS structure, and the resulting energy barrier is only 3.3 kcal/mol, which is consistent with the highly fluxional nature of IF_7.

As shown in Figure 8, the aTS and rTS structures are highly similar, with an RMSD of only 0.42 Å after alignment over all eight atoms. Both structures adopt C_{2v} symmetry, further supporting that the aTS geometry obtained from the turnstile rotation-driven relaxed scan provides a reliable initial guess for transition-state optimization. A subtle difference can nevertheless be noted in the detailed symmetry pattern: in the aTS

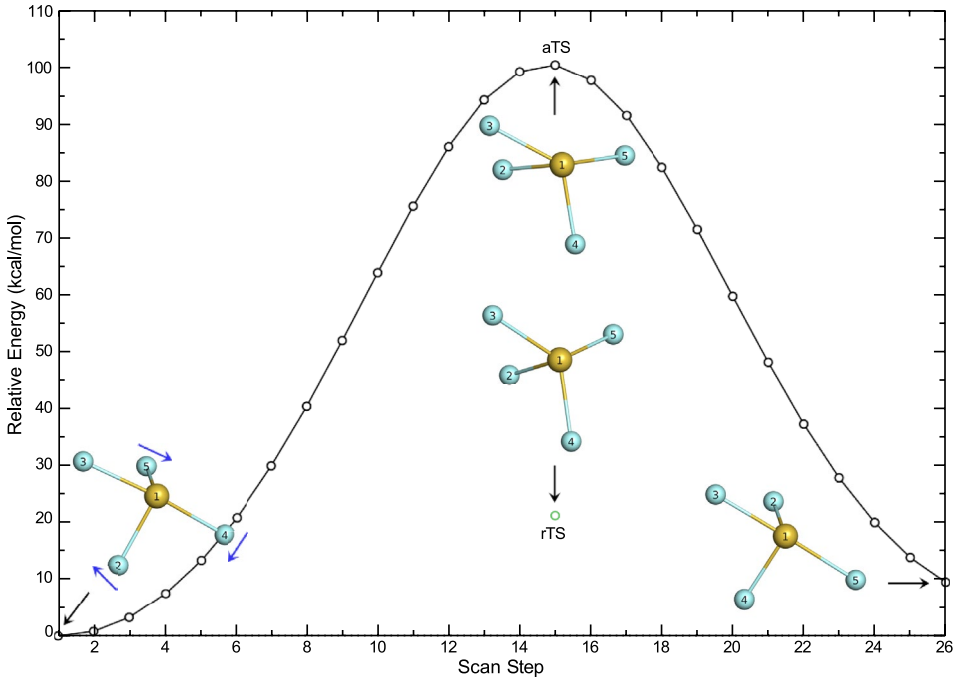

FIGURE 5 | Energy profile along the turnstile rotation driven relaxed scan path for SF_4. The first scan step corresponds to the starting structure. aTS and rTS are abbreviations for approximate and rTSs, respectively. The blue arrows in the starting structure denote the turnstile rotation direction.

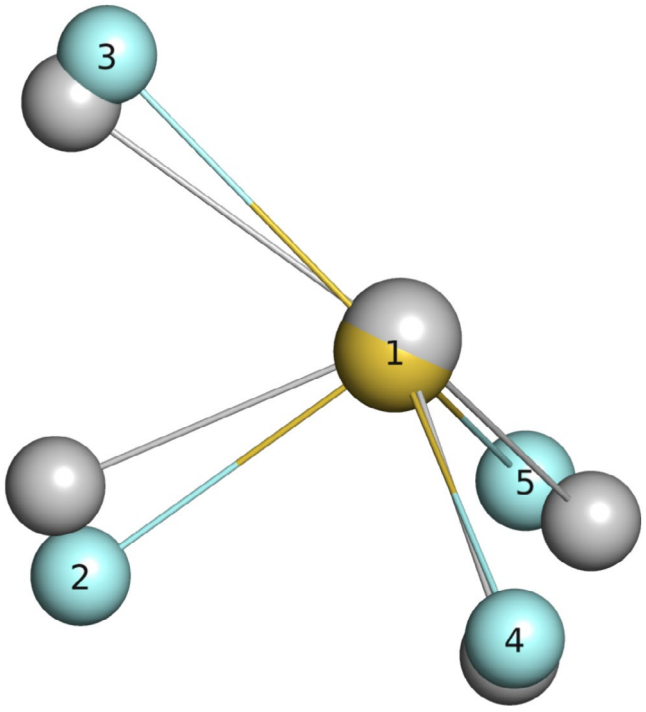

FIGURE 6 | Alignment of rTS and aTS geometries for the lever mechanism of SF_4. The rTS structure uses colored spheres (yellow and cyan) while the aTS structure uses gray color. The rTS structure takes C_{2v} symmetry where the mirror plane contains atoms 1, 2, and 3. The alignment was conducted for all 5 atoms with RMSD = 0.33 Å.

structure, the first mirror plane contains six atoms, whereas the corresponding mirror plane in the rTS structure contains only four atoms.

6.3 | Bailar Twist of Tris(Ethylenediamine) cobalt(III)

Tris(ethylenediamine)cobalt(III) is one tris-chelate metal complex first described in 1910s [29]. Its molecular structure takes D_3 symmetry in either Δ or Λ enantiomeric form. Unlike other tris-chelate metal complexes (e.g., Sc^{III}, Ti^{IV}) whose racemization mechanisms including Bailar twist and Ray-Dutt twist are well studied experimentally and theoretically, the nondissociative racemization mechanisms for Co^{III} tris chelates were not found due to the very high energy barrier of the potential racemization process according to the DFT calculations by Rzepa and co-workers [30]. We pick $[Co(en)_3]^{3+}$ as the system of interest because this compound was reported to be extremely stable as it undergoes no racemization in solution at room temperature after 3 months [31, 32]. Therefore, it is still interesting to obtain the energy barrier for the racemization mechanism in this compound although such data have been unaccessible via experiments or theoretical calculations in prior studies.

In this work, we employed the turnstile rotation driven relaxed scan workflow to study the Bailar twist motion in $[Co(en)_3]^{3+}$. As shown in Figure 9, we used the energetically optimized structure of its Λ form as the starting point. The cobalt atom is defined as the center atom and three symmetry-equivalent N donor atoms are considered as three-arm turnstile atoms. During the scanning process towards its Δ form, all six N donor atoms in the first coordination sphere are constrained during relaxation after the turnstile rotation move in each scan step.

We conducted the relaxed scan for 24 additional steps and each step rotates the turnstile motif by 5°. The energy profile climbs up to 95 kcal/mol till step 12 and gradually reaches 0 kcal/mol at

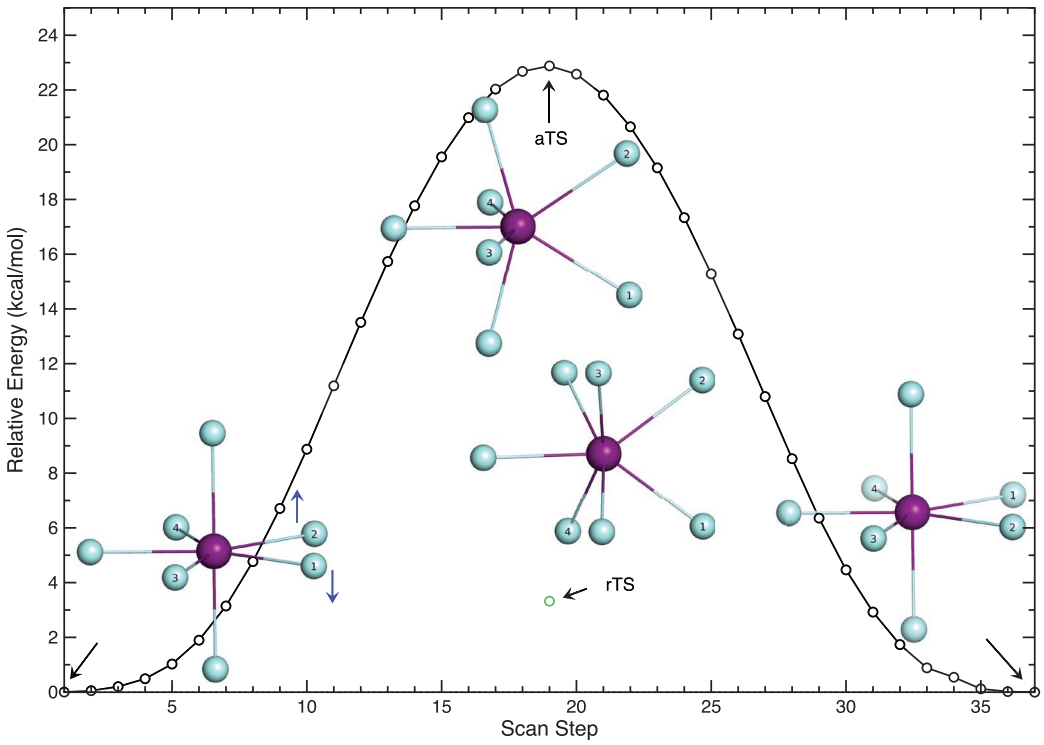

FIGURE 7 | Energy profile along the turnstile rotation driven relaxed scan path for IF_7. The first scan step corresponds to the starting structure. aTS and rTS are abbreviations for approximate and rTSs, respectively. The blue arrows in the starting structure denote the turnstile rotation direction.

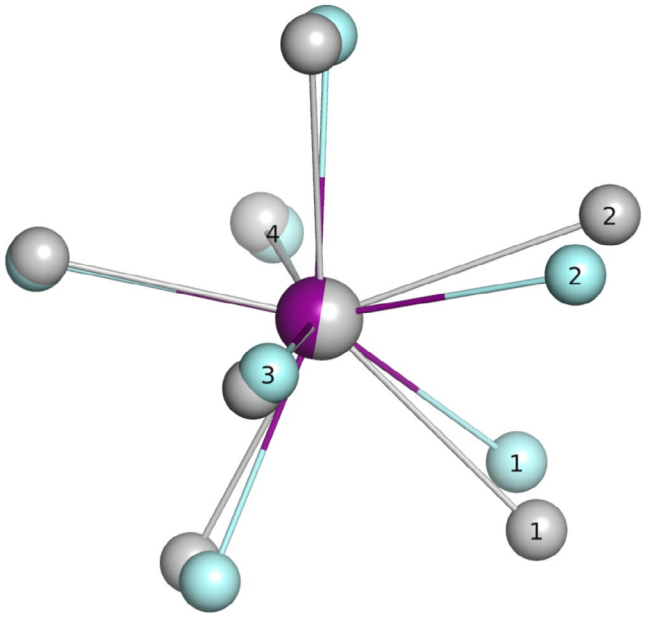

FIGURE 8 | Alignment of rTS and aTS geometries for the Bartell mechanism of IF_7. The rTS structure uses colored spheres (purple and cyan) while the aTS structure uses gray color. Both rTS and aTS structures take C_{2v} symmetry. The alignment was conducted for all 8 atoms with RMSD = 0.42 Å.

step 22. The aTS structure at step 12 takes a near-C_{3h} symmetry and the 22nd step structure returns to D_3 symmetry.

Then we used the aTS geometry as the initial guess to find the first-order saddle point (i.e., TS) on the PES and successfully found the rTS structure which is further confirmed by harmonic vibrational analysis. As shown in Figure 9, the energy barrier obtained from DFT calculations for Bailar twist is up to 57 kcal/mol which is consistent with the observation of no racemization in experiments.

We notice a large energy discrepency between the aTS and rTS points, however, this apparent anormaly falls within expectations because of the constraint used in the relaxed scan workflow. The key point here is that the aTS structure identified by this workflow is very similar to the rTS structure which is otherwise difficult to obtain.

As shown in Figure 10, we have conducted structure alignment between aTS and rTS with regard to the 7 atoms within the first coordination sphere which are constrained during scanning, the deviation is very small with RMSD = 0.27 Å.

For the Ray-Dutt twist mechanism, we also applied the turnstile rotation-driven relaxed scan workflow in an attempt to identify the aTS structure. In this case, the N donor atoms belonging to two ethylenediamine ligands were treated as two independent two-arm turnstiles and rotated simultaneously during the scan. In addition, these four N donor atoms were constrained during the subsequent geometry relaxation. Although an aTS structure could be identified along the scan profile, it did not converge to an rTS structure, that is, a first-order saddle point, upon transition-state optimization. We therefore turned to the NEB route, using the starting geometry, the approximate product geometry, and the aTS geometry as the reactant, product, and TS guess structures, respectively. The resulting reaction path reveals a dissociative mechanism involving Co-N bond

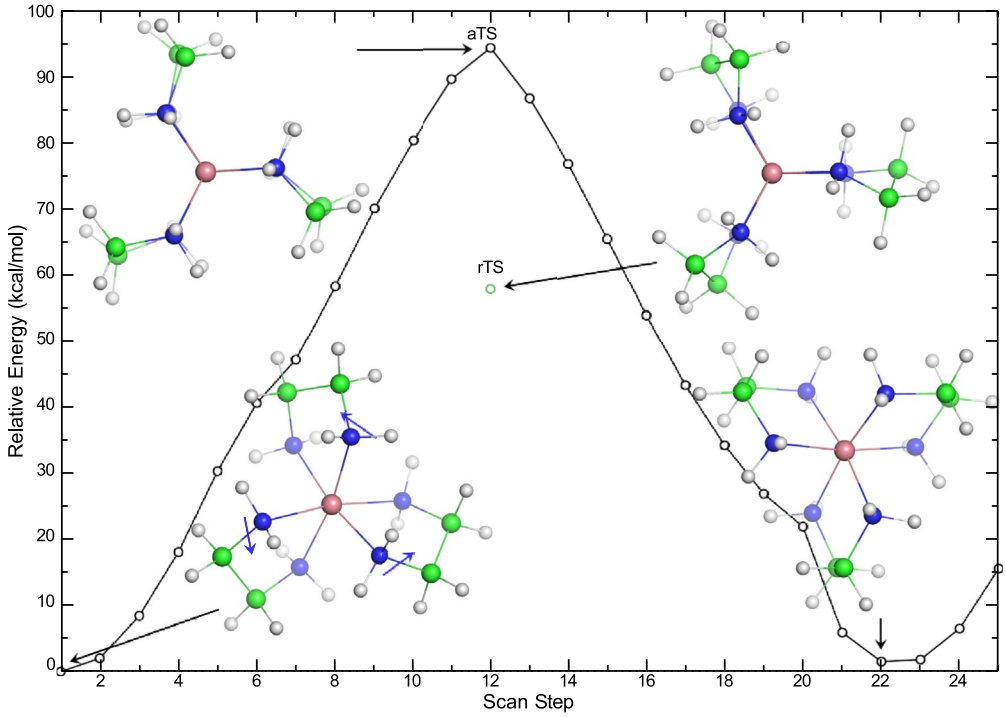

FIGURE 9 | Energy profile along the turnstile rotation driven relaxed scan path for $[Co(en)_3]^{3+}$. The first scan step corresponds to the starting structure. aTS and rTS are abbreviations for approximate and rTSs, respectively. The blue arrows in the starting structure denote the turnstile rotation direction.

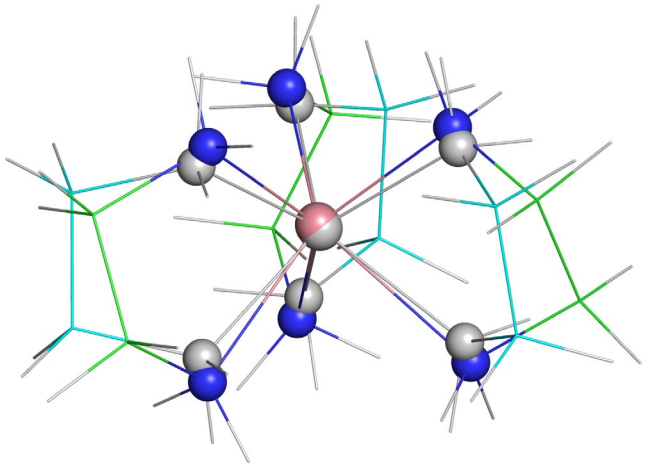

FIGURE 10 | Alignment of rTS and aTS geometries for the Bailar twist mechanism of $[Co(en)_3]^{3+}$. The central cobalt atom and first coordination sphere atoms are shown with sphere representation while the remaining atoms are shown with lines. The rTS structure uses colored spheres (salmon and dark blue) for the first coordination sphere and green color for carbon atoms in the remaining parts. The aTS structure uses gray color for the first coordination sphere and cyan color for carbon atoms in the remaining parts. The alignment was conducted for all 7 atoms within the first coordination sphere with RMSD = 0.27 Å.

cleavage followed by bond re-formation, with an energy barrier of 52.5 kcal/mol. The corresponding NEB trajectory is provided in the Supporting Information. Taken together, the high energy barriers obtained for both the Bailar twist and Ray-Dutt twist mechanisms provide a consistent explanation for the absence of racemization under ambient conditions.

6.4 | Carboxylate Arm Flipping in Bismuth Compound $[Bi^{III}(L^{NCN})(OAc)_2]$

κ^2-carboxylate is a common bidentate ligand in coordination chemistry, however, its seemingly simple arm flipping motion by 180° has received little attention.

In this example, we choose the a bismuth(III)bis(acetate) pincer complex $[Bi^{III}(L^{NCN})(OAc)_2]$ which is a DFT-predicted intermediate in the catalytic mechanism of electrochemical hydrogen evolution mediated by the bismuth pincer complex $[Bi^{III}(L^{NCN})(Cl)_2]$ first reported in our previous work [33]. As shown in Figure 11, this compound consists of a high-valent Bi(III) center coordinated to the rigid N,C,N-pincer ligand and two acetate ligands.

To study the arm-flipping motion as a turnstile rotation in the carboxylate ligand, we select the two chelating oxygen atoms from one carboxylate ligand as the two-arm turnstile atoms and drive the relaxed scan by 5° in each step starting from the energetically minimized structure. For the relaxed scan, we constrained the positions of four oxygen atoms during relaxation. The energy profile reaches the maximum (aTS) at step 19 and falls back to zero at step 37, which correspond to 90° and 180° rotation, respectively.

By using the aTS structure as the initial guess, we successfully found the rTS structure which is basically identical to the aTS structure as shown in Figure 12.

According to our calculation, the arm flipping of κ^2-carboxylate has relatively low energy barrier of 4 kcal/mol. This means it occurs almost without any barrier under ambient conditions.

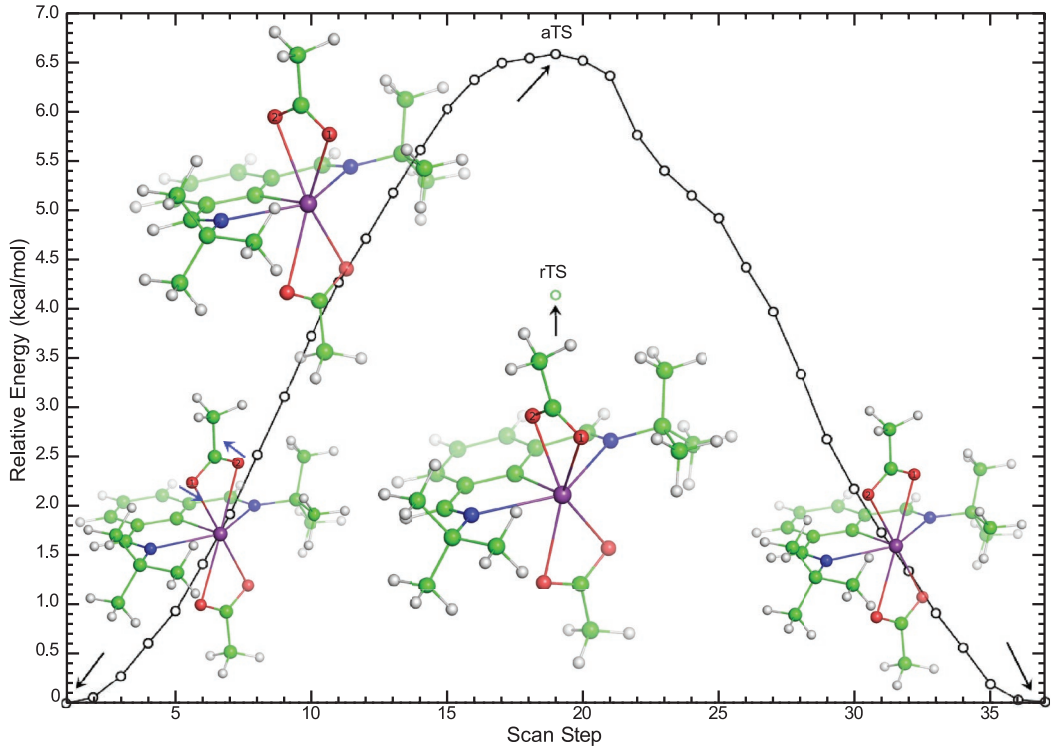

FIGURE 11 | Energy profile along the turnstile rotation driven relaxed scan path for [Bi^{III}(L^{NCN})(OAc)$_2$]. The first scan step corresponds to the starting structure. aTS and rTS are abbreviations for approximate and rTSs, respectively. The blue arrows in the starting structure denote the turnstile rotation direction.

6.5 | U-Turn-Like Rearrangement of 1,2-Benzenediselenolate Ligand in Nickel(II) Complex [Ni(bds)(dppf)]

Four-coordinate metal complexes with two bidentate ligands usually adopt tetrahedral or square-planar geometries. If one bidentate ligand is regarded as a two-arm turnstile, its twisting motion may induce a tetrahedral-to-square-planar conversion or vice versa.

In this example, we focus on the nickel(II) complex [Ni(bds)(dppf)], first reported in our previous work on dihydrogen evolution [34]. As shown in Figure 13, this compound adopts a square-planar geometry defined by two selenium atoms of the 1,2-benzenediselenolate ligand (abbreviated as bds) and two phosphorus atoms of the 1,1′-bis(diphenylphosphino)ferrocene ligand (abbreviated as dppf).

To investigate the twisting motion of the bds ligand, we started from the crystal structure of this compound (CSD entry FIMSUS) and carried out gas-phase geometry optimization. The two selenium atoms of the bds ligand were then defined as the two-arm turnstile atoms with the nickel atom as the center. The relaxed scan workflow was applied using a rotation increment of 5° per step in the direction indicated in Figure 13, while all five atoms in the first coordination sphere were constrained during the subsequent relaxation. The resulting energy profile reaches a maximum (aTS) at step 14 and a minimum at step 26. We also performed the relaxed scan in the opposite direction (see Supporting Information), but the corresponding profile suggests that rotation in that direction is thermodynamically less favorable.

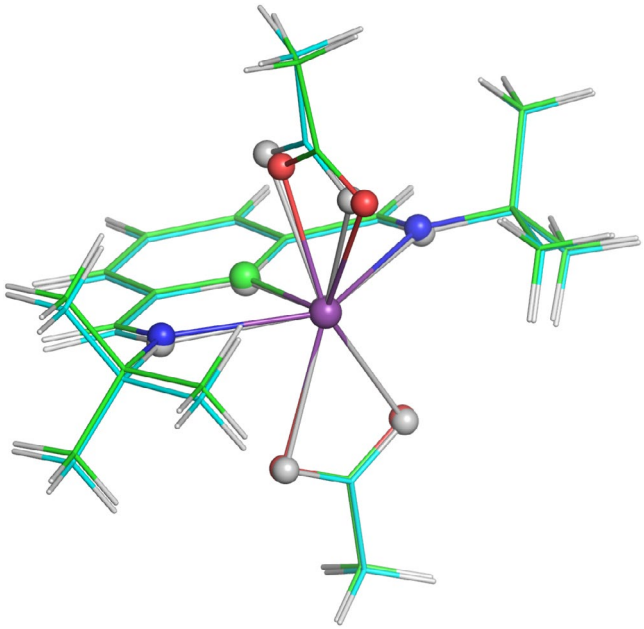

FIGURE 12 | Alignment of rTS and aTS geometries for carboxylate arm flipping mechanism in [Bi^{III}(L^{NCN})(OAc)$_2$]. The central bismuth atom and first coordination sphere atoms are shown with sphere representation while the remaining atoms are shown with lines. The rTS structure uses colored spheres (purple, red, green and dark blue) for the first coordination sphere and green color for carbon atoms in the remaining parts. The aTS structure uses gray color for the first coordination sphere and cyan color for carbon atoms in the remaining parts. The alignment was conducted for all 7 atoms within the first coordination sphere with RMSD = 0.07 Å.

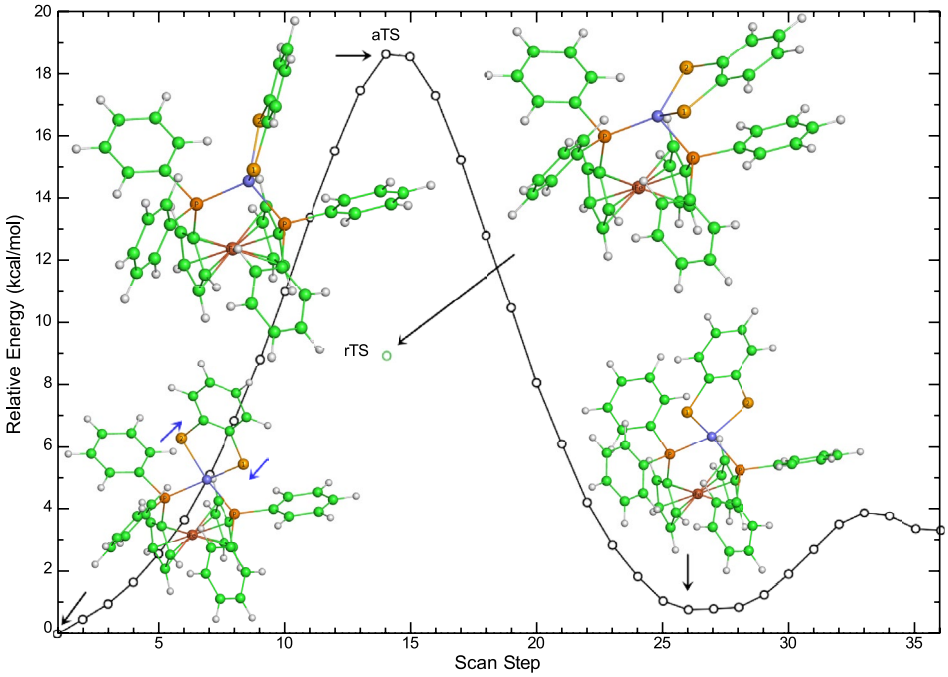

FIGURE 13 | Energy profile along the turnstile rotation-driven relaxed scan path for [Ni(bds)(dppf)]. The first scan step corresponds to the starting structure. aTS and rTS are abbreviations for approximate and rTSs, respectively. The blue arrows in the starting structure denote the turnstile rotation direction. The selenium atoms colored in orange-yellow are labeled with 1 and 2. The rTS point shown here was obtained through the NEB route followed by transition-state optimization, rather than by direct optimization starting from the aTS geometry. The energy profile for turnstile rotation in the opposite direction is provided in the Supporting Information.

To locate the rTS point on the PES, we first attempted the direct TS-refinement route by using the aTS structure as the initial guess for first-order saddle-point optimization. However, the optimized structure exhibited two imaginary frequencies rather than one. We therefore turned to the NEB route, using three structures as input: (1) the starting structure (step 1) as the reactant, (2) the step 26 structure after further geometry optimization as the product, and (3) the aTS structure as the TS guess. The resulting climbing-image (CI) structure from the NEB calculation was then used as the initial guess for transition-state optimization, leading to an rTS structure with a single imaginary frequency. This rTS structure adopts a pseudo-tetrahedral geometry and lies about 9 kcal/mol above the starting structure.

Because previous studies have suggested that nickel(II) complexes tend to prefer the high-spin state (triplet) in tetrahedral geometries and the low-spin state (singlet) in square-planar geometries, [35] we also examined the triplet-state energy of the rTS structure. We found that the singlet state is about 5.9 kcal/mol lower in energy than the triplet state, indicating that the pseudo-tetrahedral rTS structure still favors the low-spin electronic configuration.

Comparison of the aTS and rTS structures (see Figure 14) shows that in the rTS geometry the bds ligand tilts markedly toward one phosphorus atom, and this deviation from the aTS structure gives rise to the pseudo-tetrahedral arrangement. We also calculated the triplet-state energy of the aTS structure and found it to be about 3.2 kcal/mol lower than the singlet state. This observation suggests that departure from an ideal tetrahedral arrangement is an

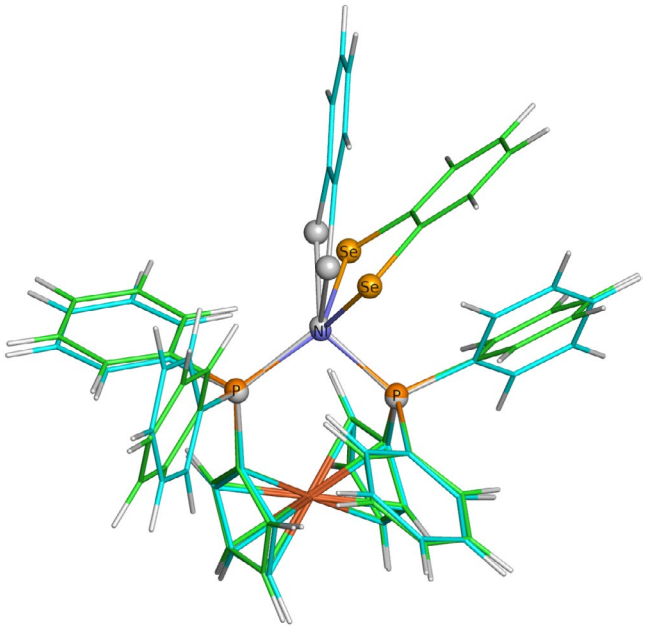

FIGURE 14 | Alignment of rTS and aTS geometries for the ligand rearrangement in [Ni(bds)(dppf)]. The central nickel atom and first coordination sphere atoms are shown with sphere representation while the remaining atoms are shown with lines. The rTS structure uses colored spheres (slate, orange, and orange-yellow) for the first coordination sphere and green for carbon atoms in the remaining parts. The aTS structure uses gray for the first coordination sphere and cyan for carbon atoms in the remaining parts. The alignment was performed using Ni and the two P atoms as references, and the resulting RMSD for all five atoms in the first coordination sphere is 0.61 Å.

important factor in stabilizing the low-spin rTS structure. A similar trend was reported by Hill and co-workers [36].

Inspection of the interpolated trajectory connecting the starting structure, the rTS, and the optimized product structure derived from step 26 reveals that the motion of the bds ligand is not a simple in-place two-arm turnstile rotation. Instead, the ligand undergoes a pronounced displacement of its center of mass near the midpoint of the nominal 180° rotation. As illustrated in Figure 15, this motion resembles a U-turn-like rearrangement rather than a conventional turnstile rotation in place.

6.6 | On the Relationship Between aTS and rTS in the TS Refinement Route

In the four showcase examples for which the direct TS refinement route was successful, the aTS and rTS structures can differ substantially in energy (see Table 2). In the IF_7 and SF_4 cases, for example, the aTS energies exceed the final rTS barrier heights by several fold. At first glance, this result may seem counterintuitive. However, such behavior is fully consistent with the design of the present workflow. During the turnstile rotation-driven relaxed scan, selected atoms in the first coordination sphere are held fixed in order to enforce the target collective motion. As a consequence, the resulting aTS structures necessarily contain additional strain associated with constrained metal–ligand interactions and ligand–ligand repulsions within the frozen region.

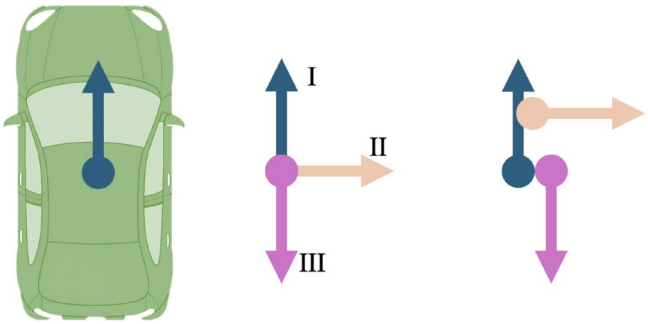

FIGURE 15 | Schematic comparison between conventional two-arm turnstile rotation and a U-turn-like rearrangement. The left panel uses a top-view car analogy to indicate molecular orientation by an arrow originating from the center of mass. This arrow symbolizes the orientation of the chelating atoms in a two-arm turnstile motif, such as the atoms labeled with 1 and 2 in Figures 11 and 13. The middle panel illustrates an in-place 180° two-arm turnstile rotation without an appreciable shift of the center of mass, as exemplified by Figure 11. The right panel illustrates a related motion accompanied by a pronounced displacement of the center of mass during the rotation, as observed for [Ni(bds)(dppf)] in Figure 13. This latter motion is referred to here as a U-turn-like rearrangement.

TABLE 2 | Summary of aTS-rTS energy gaps for the four examples successfully treated by the direct TS refinement route (kcal/mol).

Example	aTS rTS	rTS[a]	Ratio[b]
$[Co(en)_3]^{3+}$	36	58	62%
SF_4	79	21	376%
$[Bi^{III}(L^{NCN})(OAc)_2]$	3	4	75%
IF_7	20	3	593%

[a]Energy of rTS relative to the starting structure in kcal/mol.
[b]$(aTS - rTS) / rTS$.

For this reason, energetic proximity between aTS and rTS is not the primary criterion for judging the quality of an aTS structure in the TS refinement route. The more relevant criterion is structural proximity. As demonstrated by the alignments discussed above, the aTS geometries generated by the present workflow remain sufficiently close to the corresponding rTS structures to serve as high-quality initial guesses for transition-state optimization. In principle, allowing additional relaxation of selected bond lengths during the scan might reduce part of the excess strain energy. Nevertheless, the present results show that such refinement is not essential: the strain introduced during the constrained scan is readily released during the subsequent TS optimization, while the mechanistically relevant structural features of the aTS geometry are preserved.

7 | Computational Details

In this work, all quantum chemistry calculations including geometry optimization with/without constraint, harmonic vibrational frequencies, TS search [24] and NEB [25] path were performed with the ORCA 6.1.0 package [23, 37].

For the hybrid functional B3LYP calculations, the Resolution of Identity (RI) approximation for the Coulomb part combined with the Chain-of-Spheres (COSX) approximation for the exchange part (`RIJCOSX`) [38] were employed to accelerate the self-consistent field (SCF) procedure, with the `def2/J` auxiliary basis set [39] used for Coulomb fitting. For the pure meta-GGA functional M06-L calculations, only the RI approximation for the Coulomb term (`RI-J`) was applied, as no exact exchange contribution is present [38].

SCF calculations were converged using tight convergence criteria (energy change $< 10^{-8}$ E_h). Geometry optimizations and TS searches were conducted with loose convergence criteria (`LooseOpt`) to reduce computational cost.

The SF_4 and IF_7 molecules were calculated at the B3LYP/def2-SVP level, [40–44] while the cobalt, bismuth, and nickel complexes were calculated using the Minnesota meta-GGA functional M06-L [45] with Ahlrichs' def2-SVP basis set [44].

8 | Conclusions

In this work, we proposed the generalized turnstile rotation as an elementary collective motion in coordination complexes and established its explicit mathematical formulation. This definition overcomes key limitations of conventional internal coordinates, such as bond angles and dihedral angles, which often fail to provide an intuitive or systematic description of collective polytopal rearrangements. To facilitate the visualization and manipulation of such motions, we developed gTA (generalized Turnstile Assistant), a user-friendly PyMOL plugin based on

this mathematical framework, together with a versatile Python utility program, gTA-cli, for modeling turnstile rotation in molecular structures.

Building on this formulation, we introduced a practical relaxed scan workflow that combines turnstile rotation–driven coordinate driving with constrained geometry optimization. We demonstrated that this strategy efficiently generates aTS structures that serve as reliable starting points for two downstream routes toward the rTS, namely direct transition-state refinement and the NEB approach. An important advantage of this workflow is its accessibility: it can be implemented without modifying the source code of mainstream quantum chemistry packages, making it readily adaptable to diverse computational environments and amenable to future integration with machine learning potentials.

The applicability of the approach was demonstrated through five chemically diverse case studies spanning both established and previously unexplored fluxional mechanisms. We reproduced the high-barrier Bailar twist in a tris-chelate complex, reformulated the lever mechanism in SF_4 in terms of a three-arm turnstile model, and captured the low-barrier Bartell rearrangement in IF_7, illustrating the consistency of the workflow with classical mechanistic interpretations. In the bismuth pincer complex [BiIII(LNCN)$(OAc)_2$], the method revealed the low-barrier nature of the carboxylate arm-flipping process. Most notably, in the nickel(II) complex [Ni(bds)(dppf)], we identified a previously unrecognized U-turn-like rearrangement, representing a distinct turnstile-type motion accompanied by a pronounced displacement of the ligand center of mass. This analysis further uncovered a correlation between the geometric distortion associated with this rearrangement and the preference for a low-spin electronic state. Taken together, these results indicate that turnstile rotation constitutes a broadly relevant class of collective motion in coordination chemistry. By providing an explicit definition, a dedicated coordinate, and an accessible computational workflow, the present work offers a general strategy for exploring complex fluxional processes and advancing the understanding of dynamic stereochemistry in coordination and related molecular systems.

In practical terms, this framework enables the systematic generation of chemically meaningful TS guesses for concerted rearrangements that are difficult to access using conventional coordinate schemes. More broadly, it provides a foundation for integrating turnstile-driven coordinate exploration into routine mechanistic studies and automated computational workflows.

Acknowledgments

Xianlong Wang was supported by the Natural Science Foundation of Fujian Province (Grant No. 2025J01843) and Fujian Medical University (Grant No. XRCZX2017001).

Funding

This work was supported by Natural Science Foundation of Fujian Province (Grant No. 2025J01843) and Fujian Medical University (Grant No. XRCZX2017001).

Data Availability Statement

Data sharing is not applicable to this article as no datasets were generated or analyzed during the current study.

References

1. P. J. Canfield, J. R. Reimers, and M. J. Crossley, ""Polytopal Rearrangement Model of Stereoisomerization" and Its Potential as the Basis for a Systematic Model of All Stereoisomerism," *ACS Organic & Inorganic Au* 4 (2024): 356–372.

2. W. Zou, Y. Tao, D. Cremer, and E. Kraka, "Describing Polytopal Rearrangements of Fluxional Molecules With Curvilinear Coordinates Derived From Normal Vibrational Modes - A Conceptual Extension of Cremer-Pople Puckering Coordinates," *Journal of Chemical Theory and Computation* 16 (2020): 3162–3192, https://doi.org/10.1021/acs.jctc.9b01274.

3. I. Ugi, D. Marquarding, H. Klusacek, P. Gillespie, and F. Ramirez, "Berry Pseudorotation and Turnstile Rotation," *Accounts of Chemical Research* 4 (1971): 288–296.

4. P. Gillespie, P. Hoffman, H. Klusacek, et al., "Non-Rigid Molecular Skeletons—Berry Pseudorotation and Turnstile Rotation," *Angewandte Chemie International Edition* 10 (1971): 687–715.

5. E. P. A. Couzijn, J. C. Slootweg, A. W. Ehlers, and K. Lammertsma, "Stereomutation of Pentavalent Compounds: Validating the Berry Pseudorotation, Redressing Ugi's Turnstile Rotation, and Revealing the Two- and Three-Arm Turnstiles," *Journal of the American Chemical Society* 132 (2010): 18127–18140.

6. Y. Tao, W. Zou, G.-G. Luo, and E. Kraka, "Describing Polytopal Rearrangement Processes of Octacoordinate Structures. I. Renewed Insights Into Fluxionality of Rhenium Polyhydride Complex $ReH_5(PPh_3)_2$(Pyridine)," *Inorganic Chemistry* 60 (2021): 2492–2502, https://doi.org/10.1021/acs.inorgchem.0c03418.

7. Y. Tao, X. Wang, W. Zou, G.-G. Luo, and E. Kraka, "Unusual Intramolecular Motion of ReH_9^{2-} n K_2ReH_9 Crystal: Circle Dance and Three-Arm Turnstile Mechanisms Revealed by Computational Studies," *Inorganic Chemistry* 61 (2022): 1041–1050, https://doi.org/10.1021/acs.inorgchem.1c03118.

8. G. Grieco, A. Pierini, and M. Pierini, "Dynamic Processes of the First NHC-Substituted Rhenium Heptahydrides [ReH7(NHC)2]," *Dalton Transactions* 54 (2025): 13246–13256.

9. M. E. Cass, K. K. Hii, and H. S. Rzepa, "Mechanisms That Interchange Axial and Equatorial Atoms in Fluxional Processes: Illustration of the Berry Pseudorotation, the Turnstile, and the Lever Mechanisms via Animation of Transition State Normal Vibrational Modes," *Journal of Chemical Education* 83 (2006): 336, http://www.ch.ic.ac.uk/rzepa/bpr/.

10. M. J. Frisch, G. W. Trucks, H. B. Schlegel, et al., *Gaussian 16 Revision B.01* (Gaussian Inc, 2016).

11. P. J. Canfield, M. J. Crossley, J. Spreer, and S. Tillmann, "Defining Stereoisomeric Configuration Spaces and Subspaces for Arbitrary Coordination Centres ABn," ChemRxiv, 2025, https://doi.org/10.26434/chemrxiv-2025-gc7s6.

12. P. J. Canfield and M. J. Crossley, "Rigorous Treatment of Polytopal Rearrangements Reveal Surprising Complexity of Stereoisomerism Configuration Landscapes," *Chemical Science* 16 (2025): 6705–6719.

13. W. Zou, D. Izotov, and D. Cremer, "New Way of Describing Static and Dynamic Deformations of the Jahn-Teller Type in Ring Molecules," *Journal of Physical Chemistry A* 115 (2011): 8731–8742.

14. W. L. DeLano, *The PyMOL Molecular Graphics System* (DeLano Scientific, 2002).

15. L. L. C. Schrödinger, "The PyMOL Molecular Graphics System," Version 2.0, 2017.

16. M. J. Rothman and L. L. Lohr, "Analysis of an Energy Minimization Method for Locating Transition States on Potential Energy Hypersurfaces," *Chemical Physics Letters* 70 (1980): 405–409.

17. I. H. Williams and G. M. Maggiora, "Use and Abuse of the Distinguished-Coordinate Method for Transition-State Structure Searching," *Journal of Molecular Structure* 89 (1982): 365–378.

18. E. Fadrná and J. Koča, "Single-Coordinate-Driving Method Coupled With Simulated Annealing. An Efficient Tool to Search Conformational Space," *Journal of Physical Chemistry B* 101 (1997): 7863–7868.

19. M. Yang, J. Zou, G. Wang, and S. Li, "Automatic Reaction Pathway Search via Combined Molecular Dynamics and Coordinate Driving Method," *Journal of Physical Chemistry A* 121 (2017): 1351–1361.

20. M. Yang, L. Yang, G. Wang, Y. Zhou, D. Xie, and S. Li, "Combined Molecular Dynamics and Coordinate Driving Method for Automatic Reaction Pathway Search of Reactions in Solution," *Journal of Chemical Theory and Computation* 14 (2018): 5787–5796.

21. P. N. Plessow, "Efficient Transition State Optimization of Periodic Structures Through Automated Relaxed Potential Energy Surface Scans," *Journal of Chemical Theory and Computation* 14 (2018): 981–990.

22. C. Bannwarth, E. Caldeweyher, S. Ehlert, et al., "Extended Tight-Binding Quantum Chemistry Methods," *WIREs Computational Molecular Science* 11 (2020): e1493.

23. F. Neese, "Software Update: The ORCA Program System—Version 6.0," *Wiley Interdisciplinary Reviews: Computational Molecular Science* 15 (2025): e70019.

24. J. Baker, "An Algorithm for the Location of Transition States," *Journal of Computational Chemistry* 7 (1986): 385–397.

25. V. Ásgeirsson and H. Jónsson, "Nudged Elastic Band Method for Molecular Reactions: Measurement of the Reaction Path Length and Optimization of the Image Distribution," *Journal of Chemical Theory and Computation* 17 (2021): 7355–7380.

26. R. M. Minyaev and D. J. Wales, "Transition Vector Symmetry and the Internal Pseudo-Rotation and Inversion Paths of ClF_4^+," *Journal of the Chemical Society* 90 (1994): 1831–1837.

27. M. Mauksch and P. von Ragué Schleyer, "Effective Monkey Saddle Points and Berry and Lever Mechanisms in the Topomerization of SF_4 and Related Tetracoordinated AX_4 Species," *Inorganic Chemistry* 40 (2001): 1756–1769.

28. W. J. Adams, H. B. Thompson, and L. S. Bartell, "Structure, Pseudorotation, and Vibrational Mode Coupling in IF_7: An Electron Diffraction Study," *Journal of Chemical Physics* 53 (1970): 4040–4046.

29. A. Werner, "Zur Kenntnis des asymmetrischen Kobaltatoms. V," *Berichte der Deutschen Chemischen Gesellschaft* 45 (1912): 121–130.

30. H. S. Rzepa and M. E. Cass, "In Search of the Bailar and Rây-Dutt Twist Mechanisms That Racemize Chiral Trischelates: A Computational Study of Sc^{III}, Ti^{IV}, Co^{III}, Zn^{II}, Ga^{III}, and Ge^{IV} Complexes of a Ligand Analogue of Acetylacetonate," *Inorganic Chemistry* 46 (2007): 8024–8031.

31. W. Gehman and W. Fernelius, "The Mechanism of Racemization of the Tris (Ethylenediamine)cobalt(III) Cation," *Journal of Inorganic and Nuclear Chemistry* 9 (1959): 71–81.

32. A. Ehnbom, S. K. Ghosh, K. G. Lewis, and J. A. Gladysz, "Octahedral Werner Complexes With Substituted Ethylenediamine Ligands: A Stereochemical Primer for a Historic Series of Compounds Now Emerging as a Modern Family of Catalysts," *Chemical Society Reviews* 45 (2016): 6799–6811.

33. W.-C. Xiao, Y.-W. Tao, and G.-G. Luo, "Hydrogen Formation Using a Synthetic Heavier Main-Group Bismuth-Based Electrocatalyst," *International Journal of Hydrogen Energy* 45 (2020): 8177–8185.

34. Z.-H. Pan, Y.-W. Tao, Q.-F. He, et al., "The Difference Se Makes: A Bio-Inspired Dppf-Supported Nickel Selenolate Complex Boosts Dihydrogen Evolution With High Oxygen Tolerance," *Chemistry – A European Journal* 24 (2018): 8275–8280.

35. J. Krzystek, A. Ozarowski, and J. Telser, "Multi-Frequency, High-Field Epr as a Powerful Tool to Accurately Determine Zero-Field Splitting in High-Spin Transition Metal Coordination Complexes," *Coordination Chemistry Reviews* 250 (2006): 2308–2324.

36. E. A. Hill, N. Zhao, A. S. Filatov, and J. S. Anderson, "Nickel(II)-Methyl Complexes Adopting Unusual Seesaw Geometries," *Chemical Communications* 56 (2020): 7861–7864.

37. F. Neese, "The ORCA Program System," *Wiley Interdisciplinary Reviews: Computational Molecular Science* 2 (2012): 73–78.

38. F. Neese, F. Wennmohs, A. Hansen, and U. Becker, "Efficient, Approximate and Parallel Hartree-Fock and Hybrid DFT Calculations. A 'Chain-of-Spheres' Algorithm for the Hartree-Fock Exchange," *Chemical Physics* 356 (2009): 98–109.

39. F. Weigend, "Accurate Coulomb-Fitting Basis Sets for H to Rn," *Physical Chemistry Chemical Physics* 8 (2006): 1057–1065.

40. A. D. Becke, "Density-Functional Thermochemistry. III. The Role of Exact Exchange," *Journal of Chemical Physics* 98 (1993): 5648–5652.

41. C. Lee, W. Yang, and R. G. Parr, "Development of the Colle-Salvetti Correlation-Energy Formula Into A Functional of the Electron Density," *Physical Review B* 37 (1988): 785–789.

42. S. H. Vosko, L. Wilk, and M. Nusair, "Accurate Spin-Dependent Electron Liquid Correlation Energies for Local Spin Density Calculations: A Critical Analysis," *Canadian Journal of Physics* 58 (1980): 1200–1211.

43. P. J. Stephens, F. J. Devlin, C. F. Chabalowski, and M. J. Frisch, "Ab Initio Calculation of Vibrational Absorption and Circular Dichroism Spectra Using Density Functional Force Fields," *Journal of Physical Chemistry* 98 (1994): 11623–11627.

44. F. Weigend and R. Ahlrichs, "Balanced Basis Sets of Split Valence, Triple Zeta Valence and Quadruple Zeta Valence Quality for H to Rn: Design and Assessment of Accuracy," *Physical Chemistry Chemical Physics* 7 (2005): 3297–3305.

45. Y. Zhao and D. G. Truhlar, "A New Local Density Functional for Main-Group Thermochemistry, Transition Metal Bonding, Thermochemical Kinetics, and Noncovalent Interactions," *Journal of Chemical Physics* 125 (2006): 194101.

Supporting Information

Additional supporting information can be found online in the Supporting Information section. **Data S1:** The starting, aTS and rTS structures for all five showcase examples are provided in XYZ format. The ORCA .hess file of the rTS structure and the NEB trajectory for the U-turn-like rearrangement are also provided. The plugin code and workflow scripts can be found on GitHub at https://github.com/smutao/gTA-plugin and https://github.com/smutao/gTA-workflow, respectively. **Figure S1:** Energy profile along the turnstile rotation driven relaxed scan path for [Ni(bds)(dppf)] in the other direction. **Figure S2:** Normal mode displacement of imaginary frequency in the rTS structure for the U-turn mechanism in [Ni(bds)(dppf)]. This image was generated by PyVibMS plugin.